ACS OMEGA

http://pubs.acs.org/journal/acsodf

Article

Study of the Mechanical Behavior of Organic Matters Contained in Source Rocks: New Insights into the Role of Bitumen

Elshad Aslanov, Saad F. Alafnan,* Mohamed Mahmoud, Abdulazeez Abdulraheem, and Murtada Saleh Aljawad

Cite This: *ACS Omega* 2022, 7, 7024−7031

Read Online

ACCESS | Metrics & More | Article Recommendations

ABSTRACT: Assessment of mechanical properties of organic matters contained in unconventional formations is needed to understand the geomechanics of source rocks. The organic matters are part of the source rock matrix, and they are made of kerogen and bitumen. Although the literature has some studies addressing the properties of kerogen and bitumen, no apparent attempts were made to address the mechanical behavior of organic matters as a combination of both. Isolation of organic matters from the rocks for experimental assessments has some risks of altering the original properties because of their delicate nature and their existence as micro- and nanoconstituents. Some computational approaches such as molecular simulation can serve as an alternative platform for the purpose of delineating organic matter properties including the mechanical ones. This work implements available 3D molecular modeling of kerogen and bitumen with different ratios to mimic organic matters that can be investigated for the mechanical properties. Upon the recreation of different configurations of organic matters molecularly, mechanical parameters such Young's, bulk, and shear constants, as well as the stress−strain relationship for the elastic and plastic deformations were extracted. The mechanical behavior was closely monitored before and after saturation with a number of gases that are commonly found in subsurface formations such as methane, carbon dioxide, and nitrogen. The results revealed that the organic matters had a mechanical behavior envelope similar to what were reported for organic-based materials such as polymers. Moreover, the structures containing bitumen exhibited larger values of Poisson's ratio, indicating less likelihood of them to degrade upon applied stresses. The presented data substantiate the importance of accounting for both bitumen and kerogen in modeling the petrophysics and the mechanical behavior of the organic matters.

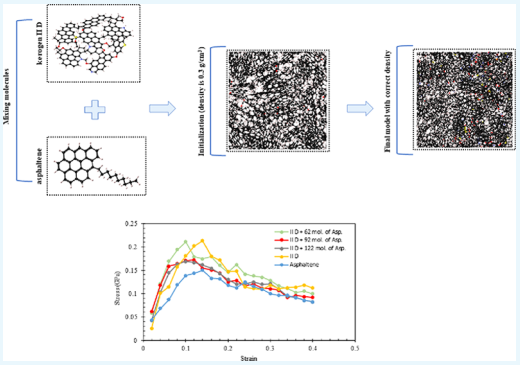

1. INTRODUCTION

The increasing demand for energy and the declining rate of production from conventional reserves necessitate the need for exploiting unconventional formations, commonly known as source rocks. Such formations require sophisticated drilling and stimulation technologies. "Unconventional" formations (self-sourcing) often refer but not limited to the shaly formations, which contain organic and inorganic constituents. The shaly formations, possessing a significant amount of natural gas, exhibit poor reservoir quality, such as permeability. Hence, commercial production requires stimulation techniques such as hydraulic fracturing to enhance the reservoir quality by creating conductive pathways inside the rock matrix, with the mechanical properties of shales being an input in the design of the fracturing process. It is difficult to determine the mechanical properties of shales due to their heterogeneity and the complex mineralogy. The current practice relies on individual assessment of all inclusions, and then, the matrix could be modeled as a whole.

The mechanical behavior of shales was investigated extensively. It was observed that the higher content of inorganic minerals leads to a higher degree of brittleness and values of elastic moduli. The increasing percentage of clay, mica, and organic matters, on the other hand, had the opposite effect.[1−4] Organic matters are inclusions existing at the micro level, and they are finely dispersed in the source rocks. They are generated from cells and tissues of biological substances such as plants, planktons, algae, and animals. The organic matters, exposed to the right conditions of pressure and temperature, are the source of hydrocarbons produced over the period of millions of years. There are various factors such as deposition, preservation, and maturation of organic matter that

Received: November 28, 2021
Accepted: February 2, 2022
Published: February 15, 2022

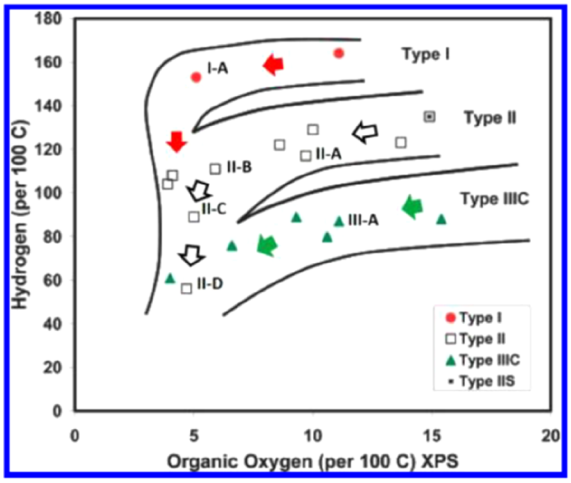

	C (%)	H (%)	O (%)
Type I	80	10.9	4.9
Type II	68.9	7.3	6.6
Type III	56.9	4.4	27.8

Figure 1. Van Krevelen diagram and elemental composition of kerogen types Reprinted with permission from [Ungerer, P.; Collell, J.; Yiannourakou, M. Molecular Modeling of the Volumetric and Thermodynamic Properties of Kerogen: Influence of Organic Type and Maturity] Copyright [**2015**] [*Energy and Fuels*].

influence the quantity and quality of end products.[5,6] The generation capacity is ultimately determined by the amount and the type of the organic matters during diagenesis, metagenesis, and catagenesis processes.[7,8] Continuous supply of organic remains carried by rivers, oxygen level, water circulation, disturbance by living organisms, sediment particles of fine-scale, and sedimentation rate are the conditions controlling the preservation of the organic matters.[9] Hydrocarbons, mainly lipid origin, form a small percentage of petroleum (10−20%). The lipid content consists of carbon homologous compounds that undergo minor structural changes during the maturation stages. This part of organic matters is more often referred to as bitumen. Bitumen is an adhesive material composed of complex hydrocarbons. Calcium, iron, sulfur, and oxygen are among the elements found in this waxy material. The properties of bitumen change with the temperature. Bitumen is rigid and brittle in low temperatures, flexible in room temperatures, and flowable in high temperatures. Consequently, bitumen tends to be mobile under the reservoir conditions of high temperature.

The second and more important component of organic matters is kerogen, which hosts a significant amount of hydrocarbons attributed to their large surface area. Kerogen serves as meso- or microporous media.[10] Based on the evolution of organic matters and elemental content (carbon, hydrogen, and oxygen), kerogens are classified into four groups: I, II, III, and IV. Type I kerogen is primarily originated from the algae and planktons that are usually deposited in lacustrine environments. This type of kerogen is immature with high hydrogen and low oxygen contents at its initial condition. The maturation of type I kerogen usually leads to the generation of waxy oils. Similarly, type II kerogen is capable of generating oil and gas under favorable subsurface conditions. This type of kerogen is rich in hydrogen and has a low concentration of oxygen. In contrast, type III kerogen has a low hydrogen and high oxygen contents, which influences its hydrocarbon generation potential. Type III kerogen is prone to produce dry gas. Kerogens of type IV are derived mainly from organic matters surviving after erosion and are present in older sediments. Weathering, combustion, and biological oxidation all play a significant role in altering kerogen content. The remaining carbon in this type of kerogen is almost entirely inert and low in hydrogen. This results in no oil or gas potential.[11−13] Figure 1 provides information about the evolution of kerogen through diagenesis, catagenesis, and metagenesis, along with the elemental composition of each kerogen type.[14]

As stated above, organic matters are the combination of kerogen and bitumen in different ratios. Usually, the latter's concentration does not exceed 20%[15] by weight in the organic matters, while the former is considered a major source of hydrocarbons. As per our knowledge, there are no existing literature on the mechanical behavior of the organic matters considering both kerogen and bitumen either experimentally or analytically. The available literature primarily focused on the properties of shale without much insights into its individual constituents, which leaves some gap in modeling the behavior as the mineralogy changes. This study investigates the mechanical properties of organic matters, represented by forming different kerogen−bitumen configurations. The kerogen type II, commonly found in shales, and asphaltene were used as representatives of kerogen and bitumen. Asphaltene is one of the major components forming bitumen.[16] Asphaltenes are high molecular weight substances found in crude oils and bitumen. Even though the exact composition of asphaltene molecules varies, the asphaltene molecule of a particular crude oil or bitumen is quite similar in its molecular structure. It appears in the core as a dark brown to black material that coats grains, filling pore spaces, and voids. Originally, asphaltenes were thought to be fragments of kerogen that had been degraded by heat. Nevertheless, we reported that asphaltenes might also be formed through condensation processes similar to those leading to kerogen.[17]

The low content of kerogen and its fine dispersion in the rock structure make experimental determination of its mechanical properties difficult. However, nanoindentation and atomic force microscopy techniques allow for the evaluation of rocks without the need for isolation. Table 1 shows information from some studies conducted for the organic matters found in different types of formations.[18−21]

On the other hand, the advancement in computational power enabled researchers to mimic the experimental processes and provides in depth insights into some nanoscale intricacies. The molecular dynamics MD approach has broad

https://doi.org/10.1021/acsomega.1c06717
ACS Omega 2022, 7, 7024−7031

Table 1. Mechanical Properties of Formations Obtained After Different Studies

study	formation	Young's modulus (GPa)	Poisson's ratio
Zeszotarski *et al.*, 2004	Woodford shale (USA)	8.8−10.4	0.1−0.4
Kumar *et al.*, 2012			
Ahmadov *et al.*, 2009 and 2011	Lockatong (USA)	10.1—13	up to 0.45
	Bazhenov (Russia)	4.7−5.9	up to 0.45
Kumar *et al.*, 2012	Kimmeridge (USA)	5	0.3
Eliyahu *et al.*, 2015	Upper Jurassic source rock (USA)	up to 25	0.3

applications in different branches of engineering to study materials such as silica, carbon nanotubes, and others.[22−25] This method is particularly advantageous in the case of organic matters, which are very sensitive and associate a risk of altering their original properties, while testing them experimentally. The first molecular representation of kerogen was introduced by Burlingame *et al.*,[26] but the model failed to capture the full chemical structure. More advanced molecular models came later.[27,28] Although the proposed models performed well in application to bitumen structures, they were found to underestimate properties of kerogen. They were restricted to the low molecular weight compounds due to technical limitations. In recent years, a greater variety of 3D structures have been developed. Studies of mechanical properties based on the available models revealed a high degree of consistency with the reported values experimentally. For instance, the outcomes of Green River shale's mechanical properties investigated by Zhang & Jamili[29] were in alignment with the experimental findings.[30] Moreover, observations made by Kashinath *et al.*[31] on Poisson's coefficients matched decently the experimental ones.

In this study, the organic matters of different kerogen to bitumen ratios are formed in a molecular simulation platform. The structures were saturated with different gases that are typically exist in the reservoir, and the mechanical behavior was thoroughly assessed before and after saturation with gases. The reminder of the paper is organized as follows: the molecular methodology including the creation of the structures, the characterization, and mechanical workflows is outlined in Section 2, which is followed by the results and discussion in Section 3. Some concluding remarks are drawn in Section 4.

2. MOLECULAR MODELING AND METHODOLOGY

2.1. Building Models. Molecular simulation is an efficient tool that has been frequently utilized in different engineering applications to infer the system's behavior under certain conditions. The basic idea behind the molecular simulation concept consists of three steps. In the first step, the molecules of the structure are positioned in the simulation box to create an initial state. This is followed by defining interaction forces, which describe repulsive and attractive forces between molecules. PCFF+ forcefield (polymer consistent forcefield plus) was used to simulate atomic interactions in this work. PCFF+ has shown an ability to reproduce properties of organic-based materials as reported by different scholars in recent studies.[32−38] Having the force field defined, the final step is to integrate Newton's equations of motion to predict particle trajectories inside the box during simulation.

MedeA software was used to conduct the molecular dynamics protocol, shown in Figure 2. This protocol allows for formation of the final condensed structure starting from a given set of macromolecules. The structures of the organic matters were built by initializing the simulation box with twelve units of type II D kerogen, introduced by Ungerer *et al.*,[37] and later by adding asphaltene molecules, known as A1, as a representative of bitumen. The asphaltene macromolecule unit used in this study was derived by Alqam *et al.*[39] Both asphaltene and kerogen units were derived from actual samples. The molar weight of every structure was taken as a base to ensure a proper mixing ratio. The chemical formulae of kerogen II D and asphaltene A1 used in this study are $S_2C_{175}N_4O_9H_{102}$ (2466 g/mol) and $C_{37}H_{33}$ (477 g/mol), respectively. Considering the molar weights of the structures, organic matters with three different kerogen to asphaltene ratios were created. It was achieved by maintaining the same number of 12 kerogen units and adding 62, 92, and 122 units of asphaltene for each calculation cycle. To avoid issues of instability that may arise in subsequent simulation steps, initialization at low density was done. As part of the molecular dynamics procedure, a 9.5 cut-off value along with a 2.0 skin is applied to the cell. An isochoric−isothermal NVT stage was conducted at the temperature of 900 K for 250 ps. Starting the simulation at high temperature would help speeding up the relaxation of the cell. Finally, three stages of NPT were performed to relax the structure by gradually reducing the temperature from 900 to 350 K isobarically at 20 MPa with the 1 fs time step (*i.e.*, 350 K and 20 MPa are deemed to be representative of typical reservoir conditions).

2.2. Porosity and Pore Size Distribution Calculation. In order to discern the degree of confinement, a detailed petrophysical characterization of the obtained structures was

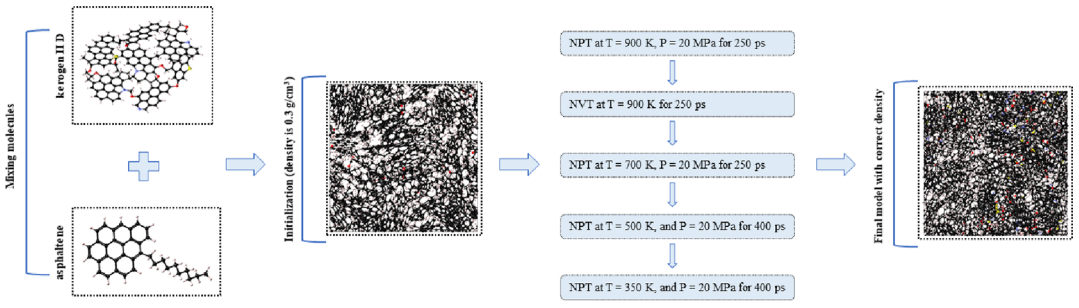

Figure 2. Visual representation of the MD protocol used to build organic matters.

https://doi.org/10.1021/acsomega.1c06717
ACS Omega 2022, 7, 7024−7031

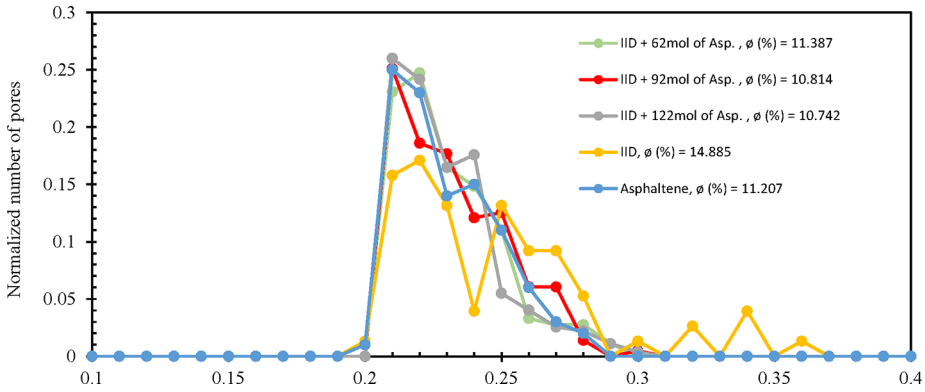

Figure 3. Pore size distribution of pure kerogen II D, pure asphaltene A1, and combination of the two at different ratios.

necessary. This was accomplished by inserting nonoverlapping spheres of a predefined threshold radius (r_i) into the void spaces within the nanoporous matrix.[40] After retrieval of each sphere (n) dimensions, the total pore volume (V_{pore}) is determined by summing them all.

$$V_{pore} = \sum_{i=1}^{n} \frac{4}{3}\pi r_i^3 \tag{1}$$

The minimum sphere radius was set to be 0.2 nm, and the frequency of radii was normalized with respect to the total number of pores obtained for each structure to extract the information about the pore size distribution. The normalization stage was necessary to establish a meaningful comparison between different structures and eliminate the size dependency because every addition of asphaltene causes an increase in size of the cubic cell.

2.3. Mechanical Properties. It is possible to determine the mechanical parameters by deforming the lattice vectors of the unit structure *via* some predefined strain. The imposed disturbance changes the total energy, which is mathematically expressed as[41,42]

$$U = \frac{E_t - E_0}{V_0} = \frac{1}{2}\sum_{i=1}^{6}\sum_{j=1}^{6} C_{ij}e_i e_j \tag{2}$$

Where U is the total energy change, E_0 is the energy before distortion, E_t is the energy after distortion, V_0 is the initial volume of the unit cell; e_i and e_j are components of the strain matrix; and C is the square Voigt stiffness matrix, which is composed of 36 elements. However, the assumption of cubic symmetry reduces the number of independent elements in the matrix to three, as shown below[43]

$$C = \begin{bmatrix} C_{11} & C_{12} & C_{12} & 0 & 0 & 0 \\ C_{12} & C_{11} & C_{12} & 0 & 0 & 0 \\ C_{12} & C_{12} & C_{11} & 0 & 0 & 0 \\ 0 & 0 & 0 & C_{44} & 0 & 0 \\ 0 & 0 & 0 & 0 & C_{44} & 0 \\ 0 & 0 & 0 & 0 & 0 & C_{44} \end{bmatrix} \tag{3}$$

The strain matrix was set up as $e = (0, 0, 0, \varepsilon, \varepsilon, \varepsilon)$ along one direction, where ε is the magnitude of strain, for the unique determination of term C_{44}

$$C_{44} = \frac{2U}{3\varepsilon^2} \tag{4}$$

In a similar manner, but by changing the direction of the applied strain, the remaining two constants can be calculated. Hence, the strain array was redefined as $e = (\varepsilon, \varepsilon, 0, 0, 0, 0)$ and $e = (\varepsilon, \varepsilon, \varepsilon, 0, 0, 0)$. This leads to the one set of system equations with two unknowns that are solved simultaneously for quantifying C_{11} and C_{12}.

$$\begin{cases} U = (C_{11} + C_{12})\,\varepsilon^2 \\ U = 3/2(C_{11} + C_{12})\,\varepsilon^2 \end{cases} \tag{5}$$

The computation of the three remaining terms of the matrix is necessary because these constants are used to estimate mechanical properties such as Poisson's ratio ν, bulk moduli K, shear moduli G, and Young's moduli E by the following relations:

$$G = \frac{5C_{44}(C_{11} - C_{12})}{8C_{44} + 6(C_{11} - C_{12})} + \frac{C_{11} - C_{12} + 3C_{44}}{10} \tag{6}$$

$$K = \frac{C_{11} + 2C_{12}}{3} \tag{7}$$

$$E = \frac{9KG}{3K + G} \tag{8}$$

$$\nu = \frac{3K - 2G}{2(3K + G)} \tag{9}$$

Continuous deformation across a given direction can be used to determine the stress−strain relationship (using eq 2). The mechanical analysis was conducted on all configurations.

3. RESULTS AND DISCUSSION

3.1. Porosity and Pore Size Distribution. Kerogen II D was found to have the highest porosity with 14.885% among all structures. Interestingly, the void fraction of organic matters decreased with the addition of new asphaltene molecules. Although the porosity of pure asphaltene (11.207%) was slightly lower compared to the initial model of organic matter (11.387%), the continuous addition of asphaltene led to porosity reduction in remaining cases. This behavior can be explained by the pore-filling effect on kerogen by asphaltene attributed to the difference in their molecular sizes. Based on the pore size distribution data given in the Figure 3, it can be deduced that pores with a radius of 0.2 to 0.25 nm were the

https://doi.org/10.1021/acsomega.1c06717
ACS Omega 2022, 7, 7024−7031

Table 2. Properties of Kerogen After the Condensing Procedure

kerogen II D	configuration 1	configuration 2	configuration 3	configuration 4
density (g/cm^3)	1.28	1.29	1.24	1.26
porosity (%)	15.2	14.4	14.7	15.1

Table 3. Properties of Organic Matters, Kerogen II D, and Asphaltene

structure	density (g/cm^3)	ø (%)	bulk (GPa)	shear (GPa)	Young's (GPa)	Poisson's (GPa)
II D + 62 mol Asp.	1.25	11.3870	4.41	0.65	1.85	0.43
II D + 92 mol Asp.	1.23	10.8140	4.4	0.5	1.46	0.45
II D + 122 mol Asp.	1.21	10.7420	4.29	0.47	1.37	0.45
II D	1.26	14.8850	3.39	0.6	1.7	0.42
asphaltene	1.14	11.2070	3.5	0.2	0.59	0.47

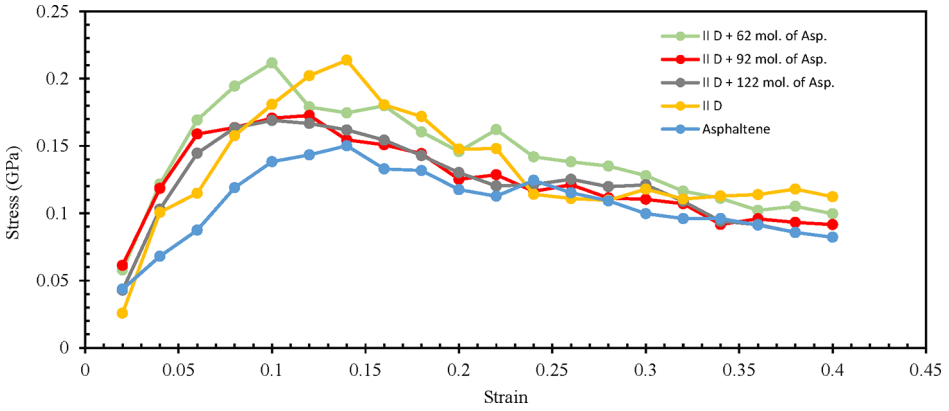

Figure 4. Stress−strain relationship of organic matters, kerogen II D, and asphaltene.

most frequent. A similar observation can be made regarding asphaltene. On the contrary, kerogen revealed the predominance of two pore size ranges between 0.2 and 0.24 nm and between 0.24 and 0.29 nm. This may indicate the presence of the dual pore system of the kerogen matrix.

3.2. Mechanical Properties and Stress−Strain Relationship. As described in the earlier section, the models of the organic matters, kerogen II D, and asphaltene A1 were formed from their respective units using the described MD protocol. The final values of density for kerogen II D (1.26 g/cm^3) and asphaltene A1 (1.14 g/cm^3) were in alignment with the values measured experimentally for the same types.

Additionally, four independent configurations of kerogen II D were created and subjected to a similar analysis to ensure robustness and the reproducibility of the followed approach. Table 2 provides information about the simulation outcomes, and it is evident that values are statistically comparable.

The stress−stain relationship behavior was obtained following the methodology covered in Section 2.3. An incremental strain of 0.02 was exerted on all units to investigate both elastic and plastic deformations. The elastic region was used to evaluate the mechanical constants. The results revealed that while shear and Young's moduli values of kerogen were almost three times higher than those of the asphaltene, the latter was more resistant to compression, as inferred from the value of Bulk moduli. Similarly, asphaltene was more prone to elongate in the direction perpendicular to the direction of the applied force, which was deduced based on Poisson's ratio. On the other hand, when it comes to the mechanical properties of the organic matters, the influence of increasing concentration of asphaltene negatively correlated with all elastic coefficients. However, this number was still higher compared to the pure state of kerogen and asphaltene. Poisson's ratio of the organic matters was not sensitive to the proportion of compounds as changes were negligible. Table 3 summarizes all findings.

The tensile deformation trend was observed to move downward, indicating a softening effect in the asphaltene (see Figure 4). The stress value for the given kerogen peaked at nearly 0.27 GPa, while asphaltene was just under 0.15 GPa for the same applied strain of 0.15. At the same time, the presence of asphaltene content with 62 molecules (the ratio is 1:1) in the matrix was found to shrink the elastic region of the structure by almost 70% compared to the kerogen. Moreover, further addition of molecules shifts the stress−strain curves of organic matters downward toward the pure asphaltene line.

Overall, the organic matter exhibits elastomer-like behavior. This occurrence is anticipated as organic matters share a similar molecular structure with polymers, represented by the long chains of repeated subunits (molecules of carbon, hydrogen, oxygen, sulfur, and nitrogen for organic matter).

The nanoindentation coupled with atomic force microscopy, as explained in the introduction, can provide in situ mapping of Young's modulus. Such data can be used as a benchmark to assess the reliability of the adopted molecular simulation. The calculated Young's modulus of kerogen II D (1.7 GPa) was found to be in close proximity to the experimentally reported values for type II kerogen (1.9—2.5 GPa).[44−47] The slight discrepancy between the lower bound in the experimental studies and the molecular simulation might be attributed to the temperature. In our case, the calculations were made at 350 K (*i.e.*, typical subsurface temperature), while the experimental ones were carried out at ambient conditions. Moreover,

https://doi.org/10.1021/acsomega.1c06717
ACS Omega 2022, 7, 7024−7031

Young's modulus and Poisson's ratio of the same kerogen type were comparable to other MD studies.[38,48]

3.3. Effect of Pore Fluid. Several scholars conducted experimental studies over the last 3 decades on the adsorption capacity of shales.[42−48] Although the primary target of this study is not adsorption-related aspects, it is vital to understand the impact of the fluids contained in kerogen micropores on the mechanical properties of organic matters. The organic matters that exist at subsurface conditions are usually saturated with gas. Although methane is the most common gas in the rock matrix, carbon dioxide and nitrogen can also be present naturally or as a result of an injection process for sequestration purposes. The condensed structure of asphaltene A1 and kerogen type II D in 1:1 (kerogen II D with 62 mol. of asphaltene) was saturated with methane, carbon dioxide, and nitrogen using Gibbs Monte Carlo simulation to investigate the influence of different fluid types adsorbed in the organic matter. The required fugacity inputs were computed through Peng-Robinson EOS with values of 35.84 MPa for methane, 16.3 MPa for carbon dioxide, and 48.94 MPa for nitrogen gas. The simulation job was performed at 350 K and 3000 psi, which was taken as a representative of the typical reservoir condition. The calculations were assisted by the Gibbs Module of MedeA environment. Figure 5 shows a visual example of the molecular simulation of adsorption on kerogen units.

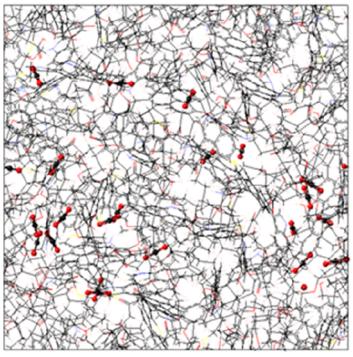

Figure 5. MD simulation mimicking the real adsorption process in kerogen. The kerogen molecular structure is shown as lines, while carbon dioxide can be visualized as ball and sticks.

It can be observed from Figure 6 that the kerogen structure tends to show a higher adsorption capacity as the number of gas molecules in all three categories was significantly higher compared to the asphaltene and the organic matter. The adsorption capacity is in alignment with the characterized porosity for all structures. The finely dispersed particles of asphaltene reduced the void spaces available in the kerogen matrix.

On the other hand, the mechanical properties of the organic matters were altered after saturation with different gases. Although Poisson's ratios remained almost the same, bulk moduli coefficients of the matrix increased following adsorption. Shear coefficients increased slightly after saturation with N_2 and CH_4 but decreased after CO_2. Young's moduli changed in the exact same manner as in the previous case (see Table 4).

Table 4. Mechanical Properties of the Organic Matter After Adsorption

property	no fluid	CH_4	CO_2	N_2
bulk (GPa)	4.41	4.68	4.62	4.6
shear (GPa)	0.65	0.68	0.59	0.7
Young's (GPa)	1.85	1.95	1.69	1.99
Poisson's ratio	0.43	0.43	0.44	0.43

Finally, the visual representation reflecting the stress−strain relationship of the organic matter saturated with fluids was shifted downward compared to the one empty of gas. The first failure point of all structures happens at 0.1 strain, but more stress corresponds to pure organic matter. However, further propagation to the failure point continues to follow a similar path for all cases, as shown in Figure 7.

4. CONCLUSION REMARKS

- The density of the organic matters represented as the mixture of asphaltene A1 and kerogen II D was close to that of the kerogen one's. Moreover, the porosity of kerogen II D was higher compared to the organic matters and pure asphaltene.
- The presence of asphaltene as part of the organic matters had a negative effect on the porosity due to the fine dispersion of asphaltene particles in the matrix.

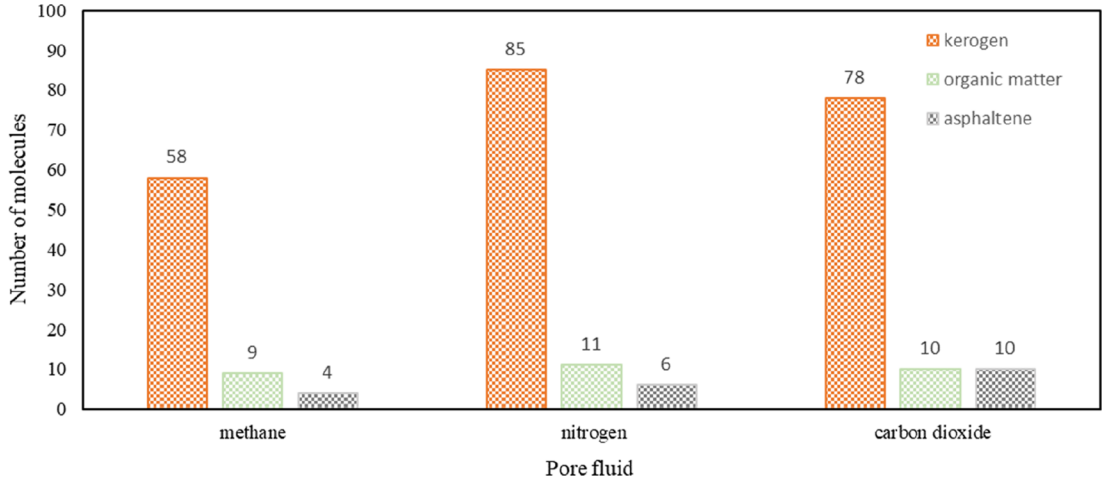

Figure 6. Number of adsorbed molecules for pure kerogen, pure asphaltene, and combination of the two.

https://doi.org/10.1021/acsomega.1c06717
ACS Omega 2022, 7, 7024−7031

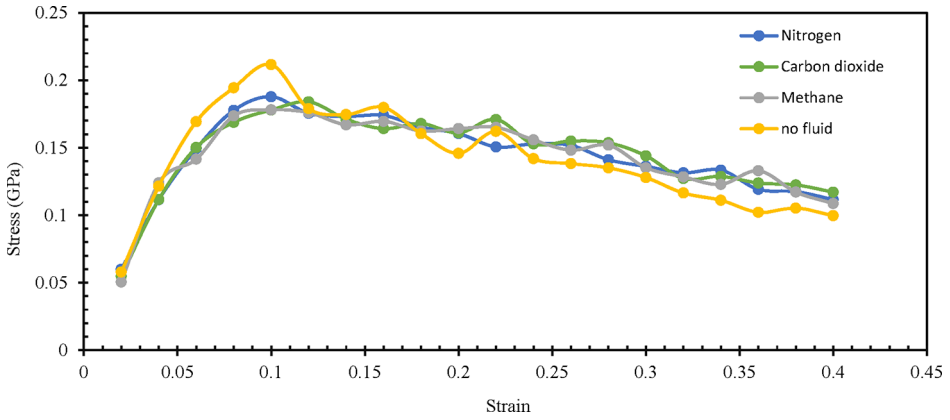

Figure 7. Stress−strain relationship of the organic matter before and after adsorption.

- Organic matters, in a general sense, exhibited both plastic and elastic deformations. The mechanical properties negatively correlated with the increasing presence of asphaltene.
- The adsorption capacity of organic matters reduced with the increasing asphaltene contents, which altered the impact of pore fluid on the mechanical behavior.
- It is recommended that the methodology outlined in this paper is repeated for other types of kerogen and bitumen. It is also recommended to verify the reported findings experimentally.

AUTHOR INFORMATION

Corresponding Author

Saad F. Alafnan − *King Fahd University of Petroleum and Minerals (KFUPM), Dhahran 31261, Saudi Arabia;* orcid.org/0000-0001-9124-8340; Email: safnan@kfupm.edu.sa

Authors

Elshad Aslanov − *King Fahd University of Petroleum and Minerals (KFUPM), Dhahran 31261, Saudi Arabia*

Mohamed Mahmoud − *King Fahd University of Petroleum and Minerals (KFUPM), Dhahran 31261, Saudi Arabia;* orcid.org/0000-0002-4395-9567

Abdulazeez Abdulraheem − *King Fahd University of Petroleum and Minerals (KFUPM), Dhahran 31261, Saudi Arabia;* orcid.org/0000-0002-9994-4436

Murtada Saleh Aljawad − *King Fahd University of Petroleum and Minerals (KFUPM), Dhahran 31261, Saudi Arabia;* orcid.org/0000-0002-3540-6807

Complete contact information is available at: https://pubs.acs.org/10.1021/acsomega.1c06717

Notes

The authors declare no competing financial interest.

NOMENCLATURES

G shear moduli, GPa
K bulk moduli, GPa
E Young's moduli, GPa
v Poisson's coefficient, dimensionless
r_i pore radius, nm.
ϕ porosity, percentage (%)
e strain array, dimensionless
C stiffness matrix
E total energy, kJ/mol

REFERENCES

(1) Nandi, A.; Conde, R. Unconfined Compressive Strength of Shale As a Function of Petrophysical Properties : A Case Study From Eastern Tennessee. *J. Tenn. Acad. Sci.* **2011**, *86*, 56−62.

(2) Rybacki, E.; Reinicke, A.; Meier, T.; Makasi, M.; Dresen, G. What Controls the Mechanical Properties of Shale Rocks?—Part I: Strength and Young's Modulus. *J. Pet. Sci. Eng.* **2015**, *135*, 702−722.

(3) Tan, J.; Horsfield, B.; Fink, R.; Krooss, B.; Schulz, H.-M.; Rybacki, E.; Zhang, J.; Boreham, C. J.; Van Graas, G.; Tocher, B. A. Shale Gas Potential of the Major Marine Shale Formations in the Upper Yangtze Platform, South China, Part III: Mineralogical, Lithofacial, Petrophysical, and Rock Mechanical Properties. *Energy Fuel.* **2014**, *28*, 2322−2342.

(4) Wanniarachchi, W. A. M.; Ranjith, P. G.; Perera, M. S. A.; Nguyen, J. T.; Rathnaweera, T. D. An Experimental Study to Investigate the Effect of Mineral Composition on Mechanical Properties of Shale Gas Formations. *51st US Rock Mechanics / Geomechanics Symposium 2017*; 2017; Vol. 3, pp 1636−1642.

(5) Mani, D.; Patil, D. J.; Dayal, A. M. Organic Properties and Hydrocarbon Generation Potential of Shales from Few Sedimentary Basins of India; Springer International Publishing, 2015; pp 99−126.

(6) Petsch, S. T.; Amherst, M. Weathering of Organic Carbon, 2nd ed.; Elsevier Ltd., 2014; Vol. *12*.

(7) Loucks, R. G.; Ruppel, S. C. Mississippian Barnett Shale: Lithofacies and Depositional Setting of a Deep-Water Shale-Gas Succession in the Fort Worth Basin, Texas. *Am. Assoc. Pet. Geol. Bull.* **2007**, *91*, 579−601.

(8) Miceli Romero, A.; Philp, R. P. Organic Geochemistry of the Woodford Shale, Southeastern Oklahoma: How Variable Can Shales Be? *Am. Assoc. Pet. Geol. Bull.* **2012**, *96*, 493−517.

(9) Tissot, B. P.; Weite, D. H. Petroleum Formation and Occurrence. A New Approach to Oil and Gas Exploration. Springer-Verlag: Berlin, 1978; p 538.

(10) Tegelaar, E. W.; de Leeuw, J. W.; Derenne, S.; Largeau, C. A Reappraisal of Kerogen Formation. *Geochim. Cosmochim. Acta* **1989**, *53*, 3103−3106.

(11) Tissot, B.; Durand, B.; Espitalié, J. Influence of Nature and Diagenesis of Organic Matter in Formation of Petroleum. *Am. Assoc. Pet. Geol. Bull.* **1974**, *58*, 499−506.

(12) Behar, F.; Vandenbroucke, M. Chemical Modelling of Kerogens. *Org. Geochem.* **1987**, *11*, 15−24.

(13) Revill, A. T.; Volkman, J. K.; O'Leary, T.; Summons, R. E.; Boreham, C. J.; Banks, M. R.; Denwer, K. Hydrocarbon Biomarkers, Thermal Maturity, and Depositional Setting to Tasmanite Oil Shales from Tasmania, Australia. *Fuel Energy Abstr.* **1994**, *58*, 3803. Geological, A. Organisation, S. 95/01310

(14) Bend, S. L. *Petroleum Geology eTextbook*; AAPG Speci (Discovery Series 11), CD-ROM, 2007.No Title.

https://doi.org/10.1021/acsomega.1c06717
ACS Omega 2022, 7, 7024−7031

(15) Dayal, A. M.; Mani, D. *Shale Gas*; Exploration and Environmental and Economic Impacts, 2017.
(16) Béhar, F.; Pelet, R. Pyrolysis-Gas Chromatography Applied to Organic Geochemistry. Structural Similarities between Kerogens and Asphaltenes from Related Rock Extracts and Oils. *J. Anal. Appl. Pyrolysis* **1985**, *8*, 173−187.
(17) Peters, K. E. Guidelines for Evaluating Petroleum Source Rock Using Programmed Pyrolysis. *Am. Assoc. Pet. Geol. Bull.* **1986**, *70*, 318−329.
(18) Ahmadov, R.; Vanorio, T.; Mavko, G. Confocal Laser Scanning and Atomic-Force Microscopy in Estimation of Elastic Properties of the Organic-Rich Bazhenov Formation. *Lead. Edge* **2009**, *28*, 18−23.
(19) Eliyahu, M.; Emmanuel, S.; Day-Stirrat, R. J.; Macaulay, C. I. Mechanical Properties of Organic Matter in Shales Mapped at the Nanometer Scale. *Mar. Pet. Geol.* **2015**, *59*, 294−304.
(20) Kumar, V.; Sondergeld, C. H.; Rai, C. S. Nano to Macro Mechanical Characterization of Shale. *Proc.—SPE Annu. Tech. Conf. Exhib.* **2012**, *4*, 3421−3443.
(21) Zeszotarski, J. C.; Chromik, R. R.; Vinci, R. P.; Messmer, M. C.; Michels, R.; Larsen, J. W. Imaging and Mechanical Property Measurements of Kerogen via Nanoindentation Burruss. *Geochim. Cosmochim. Acta* **2004**, *68*, 4113−4119.
(22) Chowdhury, S. C.; Haque, B. Z.; Gillespie, J. W. Molecular Dynamics Simulations of the Structure and Mechanical Properties of Silica Glass Using ReaxFF. *J. Mater. Sci.* **2016**, *51*, 10139−10159.
(23) Nayebi, P.; Zaminpayma, E. A Molecular Dynamic Simulation Study of Mechanical Properties of Graphene-Polythiophene Composite with Reax Force Field. *Phys. Lett. A: Gen. At. Solid State Phys.* **2016**, *380*, 628−633.
(24) Buell, S.; Van Vliet, K. J.; Rutledge, G. C. Mechanical Properties of Glassy Polyethylene Nanofibers via Molecular Dynamics Simulations. *Macromolecules* **2009**, *42*, 4887−4895.
(25) Sheikhnejad, O. Molecular Dynamic Simulation of Carbon Nanotube Reinforced Nanocomposites: The Effect of Interface Interaction on Mechanical Properties. *MOJ polym. sci* **2018**, *2*, 6−10.
(26) Burlingame, A.L.; Haug, P.A.; Schnoes, H.K.; Simoneit, B. R.; Fatty Acids Derived from the Green River Formation Oil Shale by Extractions and Oxidations1)1This review represents Part XXVII in the Series High Resolution Mass Spectrometry in Molecular Structure Studies. For Part XXVI, see A.L. Burlingame and B.R. Simoneit, Nature, in press.) — A Review. *Adv. Org. Geochem.*, Pergamon Press, 1969; 85−129. DOI: 10.1016/b978-0-08-006628-8.50008-3
(27) Oka, M.; Hsueh-Chia, C.; Gavalas, G. R. Computer-Assisted Molecular Structure Construction for Coal-Derived Compounds. *Fuel* **1977**, *56*, 3−8.
(28) Yen, T. F.; Chilingarian, G. V. Chapter 7 Structural Aspects of Organic Components in Oil Shales. *Dev. Petrol. Sci.* **1976**, *5*, 129−148.
(29) Zhang, Z.; Jamili, A. Modeling the Kerogen 3D Molecular Structure. *SPE/CSUR Unconventional Resources Conference* 2015, 1−14.
(30) Yan, F.; Han, D. H. Measurement of Elastic Properties of Kerogen. *SEG Technical Program Expanded Abstracts 2013*; 2013; pp 2778−2782.
(31) Kashinath, A.; Szulczewski, M. L.; Dogru, A. H. Modeling the Effect of Maturity on the Elastic Moduli of Kerogen Using Atomistic Simulations. *SPE/AAPG/SEG Unconventional Resources Technology Conference 2019*; 2019; pp 1−16.
(32) Afagwu, C.; Al-Afnan, S.; Patil, S.; Aljaberi, J.; Mahmoud, M. A.; Li, J. The Impact of Pore Structure and Adsorption Behavior on Kerogen Tortuosity. *Fuel* **2021**, *303*, 121261.
(33) Alafnan, S. Petrophysics of Kerogens Based on Realistic Structures. *ACS Omega* **2021**, *6*, 9549−9558.
(34) Alafnan, S.; Solling, T.; Mahmoud, M. Effect of Kerogen Thermal Maturity on Methane Adsorption Capacity: A Molecular Modeling Approach. *Molecules* **2020**, *25*, 3765.
(35) Alafnan, S.; Sultan, A. S.; Aljaberi, J. Molecular Fractionation in the Organic Materials of Source Rocks. *ACS Omega* **2020**, *5*, 18968−18974.
(36) Alafnan, S.; Falola, Y.; Al Mansour, O.; AlSamadony, K.; Awotunde, A.; Aljawad, M. Enhanced Recovery from Organic-Rich Shales through Carbon Dioxide Injection: Molecular-Level Investigation. *Energy Fuel.* **2020**, *34*, 16089−16098.
(37) Ungerer, P.; Collell, J.; Yiannourakou, M. Molecular Modeling of the Volumetric and Thermodynamic Properties of Kerogen: Influence of Organic Type and Maturity. *Energy Fuel.* **2015**, *29*, 91−105.
(38) Alafnan, S. The Impact of Pore Structure on Kerogen Geomechanics. *Geofluids* **2021**, *2021*, 4093895.
(39) Alqam, M. H.; Abu-Khamsin, S. A.; Alafnan, S. F.; Sultan, A. S.; Al-Majed, A.; Okasha, T. The Impact of Carbonated Water on Wettability: Combined Experimental and Molecular Simulation Approach. *SPE J.* **2021**, 1−13 No. August.
(40) Barber, C. B.; Dobkin, D. P.; Huhdanpaa, H. The Quickhull Algorithm for Convex Hulls. *ACM Trans. Math Software* **1996**, *22*, 469−483.
(41) Le Page, Y.; Saxe, P. Symmetry-General Least-Squares Extraction of Elastic Coefficients from Ab Initio Total Energy Calculations. *Phys. Rev. B: Condens. Matter Mater. Phys.* **2001**, *63*, 174103.
(42) Le Page, Y.; Saxe, P. Symmetry-General Least-Squares Extraction of Elastic Data for Strained Materials from Ab Initio Calculations of Stress. *Phys. Rev. B: Condens. Matter Mater. Phys.* **2002**, *65*, 104104.
(43) Jiang, D.; Wu, M.; Liu, D.; Fangfang, L.; Chai, M.; Liu, S. Structural Stability, Electronic Structures, Mechanical Properties and Debye Temperature of Transition Metal Impurities in Tungsten: A First-Principles Study. *Metals* **2019**, *9*, 967.
(44) Goodarzi, M.; Rouainia, M.; Aplin, A. C.; Cubillas, P.; de Block, M. Predicting the Elastic Response of Organic-Rich Shale Using Nanoscale Measurements and Homogenisation Methods. *Geophys. Prospect.* **2017**, *65*, 1597−1614.
(45) Wilkinson, T. M.; Zargari, S.; Prasad, M.; Packard, C. E. Optimizing Nano-Dynamic Mechanical Analysis for High-Resolution, Elastic Modulus Mapping in Organic-Rich Shales. *J. Mater. Sci.* **2015**, *50*, 1041−1049.
(46) Zhao, J.; Zhang, D.; Wu, T.; Tang, H.; Xuan, Q.; Jiang, Z.; Dai, C. Multiscale Approach for Mechanical Characterization of Organic-Rich Shale and Its Application. *Int. J. GeoMech.* **2019**, *19*, 04018180.
(47) Emmanuel, S.; Eliyahu, M.; Day-Stirrat, R. J.; Hofmann, R.; Macaulay, C. I. Impact of Thermal Maturation on Nano-Scale Elastic Properties of Organic Matter in Shales. *Mar. Pet. Geol.* **2016**, *70*, 175−184.
(48) Wu, T.; Firoozabadi, A. Mechanical Properties and Failure Envelope of Kerogen Matrix by Molecular Dynamics Simulations. *J. Phys. Chem. C* **2020**, *124*, 2289−2294.

https://doi.org/10.1021/acsomega.1c06717
ACS Omega 2022, 7, 7024−7031